Report No. NAWCADWAR-92029-60

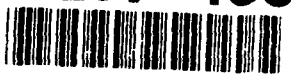

MELT SPINNING OF INTERMETALLIC ALLOYS: HEAT TRANSFER AND MICROSTRUCTURE

Jim S.J. Chen (Temple University)
William E. Frazier (NAWCADWAR)
Air Vehicle and Crew Systems Technology Department (Code 6063)
NAVAL AIR WARFARE CENTER - AIRCRAFT DIVISION
Warminster, PA 18974-0591

21 APRIL 1992

FINAL REPORT
Period Covering September 1991 to April 1992
Task No. 1
Work Unit No. ZP180
Program Element No. 62234N
Project No. R534A57

Approved for Public Release; Distribution is Unlimited.

Prepared for
Air Vehicle and Crew Systems Technology Department (Code 60C)
NAVAL AIR WARFARE CENTER - AIRCRAFT DIVISION
Warminster, PA 18974-0591

NOTICES

REPORT NUMBERING SYSTEM — The numbering of technical project reports issued by the Naval Air Warfare Center, Aircraft Division, Warminster is arranged for specific identification purposes. Each number consists of the Center acronym, the calendar year in which the number was assigned, the sequence number of the report within the specific calendar year, and the official 2-digit correspondence code of the Functional Department responsible for the report. For example: Report No. NAWCADWAR-92001-60 indicates the first Center report for the year 1992 and prepared by the Air Vehicle and Crew Systems Technology Department. The numerical codes are as follows:

CODE	OFFICE OR DEPARTMENT
00	Commanding Officer, NAWCADWAR
01	Technical Director, NAWCADWAR
05	Computer Department
10	AntiSubmarine Warfare Systems Department
20	Tactical Air Systems Department
30	Warfare Systems Analysis Department
50	Mission Avionics Technology Department
60	Air Vehicle & Crew Systems Technology Department
70	Systems & Software Technology Department
80	Engineering Support Group
90	Test & Evaluation Group

PRODUCT ENDORSEMENT — The discussion or instructions concerning commercial products herein do not constitute an endorsement by the Government nor do they convey or imply the license or right to use such products.

Reviewed By: J. Waldman Date: 24 Aug 92
Branch Head

Reviewed By: D L Shaffer Date: 9/9/92
Division Head

Reviewed By: L H Trost Date: 7 Sep 92
Director/Deputy Director

REPORT DOCUMENTATION PAGE

Form Approved
OMB No. 0704-0188

1. AGENCY USE ONLY (Leave blank)	2. REPORT DATE	3. REPORT TYPE AND DATES COVERED
	21 April 1992	Final 9/91 - 4/92

4. TITLE AND SUBTITLE
Melt Spinning of Intermetallic Alloys: Heat Transfer and Microstructure

5. FUNDING NUMBERS
PE 62234N
PN R534A57
TA 1
WU ZP180

6. AUTHOR(S)
Jim S.J. Chen (Temple University)
William E. Frazier (NAWCADWAR)

7. PERFORMING ORGANIZATION NAME(S) AND ADDRESS(ES)
Air Vehicle and Crew Systems Technology Department
(Code 6063)
NAVAL AIR WARFARE CENTER - AIRCRAFT DIVISION
Warminster, PA 18974-0591

8. PERFORMING ORGANIZATION REPORT NUMBER
NAWCADWAR-92029-60

9. SPONSORING/MONITORING AGENCY NAME(S) AND ADDRESS(ES)
Air Vehicle and Crew Systems Technology Department
(Code 60C)
NAVAL AIR WARFARE CENTER - AIRCRAFT DIVISION
Warminster, PA 18974-0591

10. SPONSORING/MONITORING AGENCY REPORT NUMBER

11. SUPPLEMENTARY NOTES

12a. DISTRIBUTION/AVAILABILITY STATEMENT
Approved for Public Release; Distribution is Unlimited.

12b. DISTRIBUTION CODE

13. ABSTRACT *(Maximum 200 words)*

Analyses and experiments are performed to investigate heat transfer in melt spinning of intermetallic materials. Previous research efforts in the modeling, the analysis, and the measurement of melt spinning processes are reviewed. The importance of the process parameters including melt temperature, melt pouring rate, wheel temperature, spinning speed, nozzle-to-wheel gap, and thermal properties of ribbon and wheel are addressed. A one-dimensional transient mathematical model is developed to predict thermal behavior of melt spinning. The solid-liquid interface velocity and the cooling rate for melt spun Al_3Ti are presented. The significance of solidification rate is demonstrated by comparing the macrostructure and microstructure of a rapidly solidified Al_3Ti ribbon with a conventionally solidified ingot of the same composition.

14. SUBJECT TERMS
Melt Spinning, Solidification
Intellegent Processing

15. NUMBER OF PAGES

16. PRICE CODE

17. SECURITY CLASSIFICATION OF REPORT	18. SECURITY CLASSIFICATION OF THIS PAGE	19. SECURITY CLASSIFICATION OF ABSTRACT	20. LIMITATION OF ABSTRACT
UNCLASSIFIED	UNCLASSIFIED	UNCLASSIFIED	SAR

CONTENTS

FIGURES

TABLES

Nomenclature

A	cooling surface area
c	specific heat
d	gap between crucible and wheel
D	mass diffusion coefficient of the solute
h	local heat transfer coefficient
k	thermal conductivity of the strip, W(m·K)
L	latent heat of fusion
Pr	Prandtl number (=ν/α)
q	local heat flux
Q	overall heat transfer rate
s	solidification thickness (see Fig. 3)
t	time
T_i	initial temperature of molten metal
T_L	liquidus temperature of alloy
T_m	melting temperature of ribbon
T_o	ribbon/wheel contact temperature
T_S	solidus temperature of alloy
T_w	bulk wheel temperature
U	wheel spinning speed
x	Lagrangian coordinates, defined in Fig. 3
V_j	jet velocity of molten metal

Greek symbols

α	thermal diffusivity
β	a dimensionless parameter defined in Eq. (7)
δ	dendrite arm or cell spacing
λ	a dimensionless parameter defined in Eq. (13)
ν	kinematic viscosity of liquid
ρ	density of

Subscripts

1	ribbon
2	wheel
L	liquid
S	solid

FOREWORD

This report is based on the collaborative effort of Jim S.J. Chen (Temple University), and William E. Frazier (NAWCADWAR), during the period of September 1991 to March 1992. Dr. Chen is an associate professor in the Department of Mechanical Engineering at Temple University. Through the ASEE-NAVY Sabbatical Leave Program, he was appointed to conduct research at the Advanced Metallic and Ceramics Branch, Naval Air Warfare Center, Aircraft Division, Warminster, PA, for the period of December 1991 to August 1992. In collaboration with Dr. Frazier, Dr. Chan is working primarily on the melt spinning process at the NAWCADWAR during his Sabbatical Leave. This program is administered by Mr. Tim Turner of the American Society of Engineering Education, Dr. D. Polk of the Office of Naval Research, and Ms. Carol Vanwyk of the NAWCADWAR. Dr. Jeffrey Waldman is the head of the branch in which this research is conducted. Professor Ampere A. Tseng's, Drexel University, technical guidance is also acknowledged.

INTRODUCTION

In the last twenty years, rapid solidification processing (RSP) has emerged as a means of producing new materials with favorable mechanical, electrical, and corrosion-resistant properties. The high cooling rates achieved during RSP can produce amorphous alloys[1] and alloys having very fine and homogeneous microstructures by extending the solid state solubility of the solute[2,3]. Table 1 lists the range of cooling rates in a variety of solidification processes. The term of "rapid" solidification is designated for cooling rate in the range of 10^3 -10^9 K/s. Since the segregation (i.e., the dendrite arm spacing) decreases as the cooling rate increases, finer microstructures are produced. Numerous techniques have been developed to produce rapidly solidified alloys including laser heating, atomization, and melt spinning. In this study, we are concerned with heat transfer in melt-spinning-based rapid solidification of intermetallic materials.

Table 1. Range of Cooling Rates in Solidification Processes

Process	Cooling Rate (K/s)	Dendrite Arm spacing (μm)	Desig-nation
large sand casting and ingots	10^{-4}-10^{-2}	5000-200	slow
continuous casting	10^{-2}-10^{1}	200 - 50	medium
die casting; roll casting; spray casting; thin strip casting	10^{1} -10^{3}	50 - 5	high
melt spinning; fine powder atomization; laser heating	10^{3}-10^{9}	5 - 0.05	rapid

The development of high performance aircraft structures and propulsion systems demands the implementation of newly emerging materials such as titanium aluminides and other intermetallic alloys[4,5]. These materials must possess good mechanical and corrosion-resistant properties at high temperatures (900°C or higher). A major problem encountered in solidification of these intermetallics is the segregation of the constituents. **Rapid solidification processing (RSP)** appears to be a viable technique capable of producing homogenous microstructure of stoichiometric or non-stoichiometric intermetallics.

In melt spinning, the molten metal is brought into contact

with a rapidly-rotating wheel. The liquid metal is cooled by the wheel and is rapidly solidified. Extremely high cooling rates may suppress the nucleation of a crystalline solid. The resulting material is known as metallic glass for which the glass transition temperature and the crystallization temperature may be identified. For crystalline materials, melt spinning may curtail or eliminate the formation of unfavorable phases. Melt spinning may be further classified according to the method of pouring liquid metal onto the spinning wheel. Fig. 1(a) shows the **free jet melt spinning** in which the crucible nozzle is located relatively far away from the wheel. In this method, Rayleigh and capillary instabilities may arise from disturbances to the jet free surface. The method was later modified in **planar flow casting as shown in** Fig. 1(b) in which the molten metal is introduced under pressure and the nozzle is brought very close to the wheel. The planar flow casting leads to improved stability and better control of the flow and to the ability of producing wider ribbons up to 4-6 inches. A third method is called **melt extraction** as shown in Fig. 1(c) wherein the spinning wheel (the moving heat sink) is brought into contact with the surface of the molten metal and a thin layer of liquid is dragged out by the spinning wheel. At NAWC/AD (Naval Air Warfare Center/Aircraft Division), an arc melt spinner (Fig. 2) is used to produce intermetallic materials. This method employs a hybrid scheme combining the planar flow casting and the melt extraction methods.

The objectives of this paper are threefold. First, previous efforts in modeling and measurements of fluid flow and heat transfer of RSP by melt spinning are reviewed. Secondly, a simplified heat transfer analysis of RSP by melt spinning is developed and effects of process variables on solidification are discussed. Thirdly, a stoichiometric intermetallic (Al_3Ti) is processed by melt spinning and mold casting and their resulting microstructures are compared.

PREVIOUS RESEARCH

It is known that the microstructures of the rapidly solidified materials are influenced by the cooling rate, the solidification rate, and the degree of undercooling. Some researchers have modeled complicated fluid flow and heat transfer phenomena in melt spinning to predict the cooling rate and the propagation velocity of the solid/liquid interface. Other researchers are more concerned with the microstructures[6] and mechanical properties of the materials produced, and therefore, prefer simplified heat transfer models. This requires interdisciplinary research to develop processing/microstructure /property relationships and to optimize the process capable of producing precisely controlled and reproducible microstructure.

Depending on the relative efficiency of the heat and momentum

transfer, two ribbon formation mechanisms have been proposed: (a) the momentum controlled mechanism and (b) the thermally controlled mechanism. Attempts to model coupled momentum and heat transfer are in progress. In general, the puddle shape and ribbon thickness are controlled by momentum transfer including process variables such as the pouring rate, the spinning speed, and the nozzle/wheel gap. Properties such as viscosity and surface tension, both of which are temperature dependent, affect significantly the puddle stability, surface waves, and contact angles. On the other hand, the cooling rate and the solidification rate are controlled by heat transfer. Process variables such as the melt temperature, the wheel temperature, and the materials' thermal properties govern the solidification rate.

In momentum controlled models, the fluid flow of the molten metal including boundary layer, streamlines, contact angle, and free surface is considered. Gutierrez and Szekely[7] have developed a mathematical model of the planar flow casting process. This model is based on the principles of lubrication theory and capillary fluid dynamics. However, the momentum equation in their model is only valid for fully developed flow between two parallel plates. Takeshita and Shingu[8] have developed an analysis of the melt puddle shape and circulation. A computer program is used to solve two-dimensional transient fluid flow with free boundaries, but it fails to include heat transfer and solidification. A mathematical model for melt-spinning based on a two-dimensional steady-state condition has been developed by Berger and Ai[9]. Their analyses follow a simplified control volume approach in which overall conservation laws for mass, momentum, and energy are satisfied for each of the zones into which the flow field can be conveniently subdivided. The zones are the reservoir, the nozzle, the liquid pool, and the solidified thin metal sheet. The conservation laws can be solved to yield the thickness of the sheet with the reservoir pressure, the ambient pressure, the nozzle/drum gap, the drum speed, and the geometry as input parameters. Although this leads to physical insight into the process, the solution of this control volume approach is only qualitative. Further, the interface heat transfer was not considered in the analysis. These studies show that the ribbon thickness is strongly affected by the gap (d) between the crucible and the spinning wheel. The ribbon thickness in the range of 0.1 to 0.2 d has been reported. Kavesh[10] reported that the ribbon thickness is proportional to $V_j^m U^n$, where V_j and U are the melt velocity and wheel speed respectively. Typical values of m and n are 0.25 and -0.75 respectively.

In thermally controlled models, heat diffusion is considered to control the solidification, since the thermal diffusion rate exceeds the momentum diffusion rate by two orders of magnitude for liquid metals, i.e., $Pr = \nu/\alpha = O(10^{-2})$. Vogt[11] measured the ribbon surface temperature by means of high-speed infrared pyrometer. A 1-D finite difference heat transfer and

solidification model based on Lagrangian coordinates was used to interpret the cooling curves. The interface heat transfer coefficient was found to be in the range of 0.7 to 1.3 x 10^6 W/m^2 K in the initial ribbon/wheel contact area. Towards the end of the puddle where ribbon/wheel interface heat transfer coefficient is significantly reduced, the heat transfer is nearly described by Newtonian cooling. Using a similar technique, Muhlbach et al.[12] reported the local heat transfer coefficient near the initial puddle/wheel contact is 10^8 W/m^2 K. Both aforementioned studies concluded that the ribbon formation mechanism is thermally controlled for crystalline materials. Recently, Wang and Matthys[13] modeled the planar flow casting of pure metals using a control volume integral method in which the heat transfers for both ribbor and wheel are considered. The results include the cooling rate as well as the solid/liquid interface velocity.

EXPERIMENTAL PROCEDURES

As shown in Fig. 2, the Aircraft Division of the Naval Air Warfare Center (NAWC/AD, formerly NADC) is equipped with a Tungsten Arc Melt Spinner, which is capable of producing melting temperatures up to 3000°C. In order to minimize the reactions of the intermetallic alloys such as titanium aluminides with the surrounding atmosphere, it utilizes a tilting water-cooled copper hearth and the apparatus is in a 5 psi Argon environment. The 10-inch (diameter) spinning wheel is made of molybdenum for its high melting temperature and hardness. An AC motor with a variable speed controller can control the spinning speed from 300 - 3000 rpm. The arc power is controlled via a DC power generator rated at 44 volts/1000 amps converted from an ac input at 480 volts/3 phases/100 amps. The geometric configuration of the Marko Materials Inc.,model 2T melt spinner differs significantly from conventional jet casting and planar flow casting systems. The molten metal is introduced to the wheel at the "9 o'clock" position by tilting the hearth and allowing the metal to be extracted.

In this experiment, 0.25 kg of stoichiometric Al_3Ti was made by arc melting 99.99% pure aluminum and 99.8% pure titanium. In order to achieve material uniformity, the ingot was turned and remelted three times before melt spinning. The crucible pouring tip is 1 mm away from the wheel surface. The wheel, the arc electrode, and the crucible are all located in a vacuum chamber. The chamber was evacuated to 10 microns by a mechanical pump and then to 5 x 10^{-6} torr by a diffusion pump. Argon was then fed to the chamber to 5 psia. The casting wheel was turned on to a speed of 2030 rpm or a casing speed of 27 m/s prior to melting. The tungsten electrode was then turned on to melt the aluminum and titanium. The electrode tip was moved around to improve homogeneous mixing of the molten alloys. After the ingot was fully molten, the arc intensity is adjusted to maintain a stable molten pool in the hearth. The crucible was gradually tilted so that the

molten metal flows over the notched tip of the hearth and makes contact with the rim of the rotating wheel to form rapidly solidified ribbons. Due to its brittleness, the titanium aluminide in the form of filament or ribbon break off into short segments. The solidified ribbons have lengths of 5 - 15 mm, widths of 0.5 - 1.5 mm, and thicknesses in the range of 50 - 100 μm. The short ribbon length is partially attributed to the brittle nature of Al_3Ti.

In conducting the experiments, it was found that at high wheel speed the melt splashes off the puddle and at too low speed the solidified ribbon may get jammed in the gap. Increasing wheel speed generally decreases the ribbon thickness but increases the cooling rate. It was also found that tilting the crucible at a lower rate results in more stable puddle and therefore longer ribbon and less porosity. In all ribbons, significant surface ripples and porosity were observed indicating a large portion of ribbon/wheel interface is not in good contact. This is partially attributed to surface wetting and dynamic contact angle. Generally, bright surfaces are noticed on the free surface side and dull surfaces are observed on the ribbon/wheel contact side.

Kroll's reagent was used to etch the polished specimens for optical examination. Differential thermal analysis (DTA) was used in order to ascertain the temperature of various phase relationships, e.g., the alloy's melting temperature. Experiments were conducted using a DuPont 1090 thermal analysis unit. The specimens were heated from 25°C to 1600°C at 20°C/min. in a dry helium atmosphere and allowed to cool to room temperature. The experiment was repeated using the same sample in order to curtail the effects of metastable phase transformation.

PROCESS MODELLING

A complete process model must consider the fluid flow, the heat transfer, and the solidification process (including microstructure modeling). Momentum transfer governs the liquid flow and puddle formation, heat transfer controls the cooling rate and thus the solidification thickness and the solidification rate, and mass transfer governs the distribution of the solute and dendrite growth. Based on diffusion theory, the laminar boundary layer thickness, the solidified ribbon thickness, and the dendrite arm spacing are found to be proportional to $(\nu t)^{1/2}$, $(\alpha t)^{1/2}$, and $(Dt)^{1/2}$, respectively. In the case of pure metals, exact solutions exist in the absence of convention in the liquid[14,15].

Assuming the thermally controlled mechanism and using a Lagrangian coordinate (moving at the same speed as the wheel surface), the heat transfer equations for the wheel (substrate) and the ribbon alloy (e.g, Al_3Ti) in Fig. 3 are,

$$\rho_1 C_1 \frac{\partial T_1}{\partial t} = \frac{\partial}{\partial x}\left(k_1 \frac{\partial T_1}{\partial x}\right) + \rho_1 L \frac{\partial f}{\partial t} \quad (1)$$

$$\rho_2 C_2 \frac{\partial T_2}{\partial t} = \frac{\partial}{\partial x}\left(k_2 \frac{\partial T_2}{\partial x}\right) \quad (2)$$

Where t is time, T is the temperature, ρ is the density, c is the specific heat, k is the thermal conductivity, L is the latent heat of solidification, and f is the solidified fraction of ribbon. The subscripts "1" and "2" represent the ribbon and the wheel respectively. The boundary condition at the interface is based on the interface heat transfer coefficient, h

$$k_1 \frac{\partial T_1}{\partial x} = k_2 \frac{\partial T_2}{\partial x} = h\,(T_1 - T_2) \quad (3)$$

Here, the interface heat transfer coefficient between the ribbon and the wheel is critical in determining the cooling and solidification rates. The local values of h were found to vary from 10^8 W/m^2 K in the liquid/wheel contact region to 10^4 W/m^2 K in the solid/wheel contact region[12]. Vogt[11] reported typical h values in the range of 10^5 to 10^6 W/m^2 K. Equation (1) may be rearranged as,

$$\rho_1 \left(C_1 - L\frac{\partial f}{\partial T}\right) \frac{\partial T_1}{\partial t} = \frac{\partial}{\partial x}\left(k_1 \frac{\partial T_1}{\partial x}\right) \quad (4)$$

and

$$\begin{array}{ll} f = 0 & (\textit{liquid region}) \\ f = f\,(T) & (\textit{mushy region}) \\ f = 1 & (\textit{solid region}) \end{array} \quad (5)$$

where f as a function of temperature may be based on equilibrium and non-equilibrium thermodynamics[16]. The term in the parenthesis of the left hand side of Eq. (4) is often referred as the effective specific heat which is significantly higher than c_1 in the mushy region. During the melt spinning process, heat is rapidly removed from the molten metal. Nucleation of the first solid phase generally occurs at temperatures substantially below the alloy's equilibrium melting temperature, which is referred as undercooling. Levi and Mehrabian[17] found that for undercooled metal droplets that solidification velocities were initially rapid, the droplet absorbs most of the latent heat of fusion and heat extraction from the powder particle plays a minor role. As solidification progresses, the heat flux from the powder can not keep pace with the heat generated from the latent heat of fusion. The solidification velocity slows and is dominated by the rate of

heat extraction from the particle. Therefore, the majority of solidification proceeds at a fixed temperature below the liquidus temperature[18].

The temperature distributions at two downstream cross sections (see Fig. 3) of the initial puddle/wheel contact are shown in Fig. 4. At the initial contact, the wheel and the liquid at x=0 reach an equilibrium temperature at T_o. The upper portion in Fig. 4 shows the temperature distribution of the liquid and the wheel at the cross section A-A' shortly after the contact is made. Although the liquid at the contact surface reduces to a temperature below the liquidus temperature, the solidification is delayed due to undercooling. Further downstream at B-B' the solidification is begun and propagates in the x direction. The temperature distribution is shown in the lower portion of Fig. 4. The thermal layer in the wheel increases due to thermal diffusion. The ribbon consists of a solid region, a mushy region, and a liquid region. In general, the temperature curves are continuous, but the temperature gradients are not. In the liquid region near the mushy region, the temperature is below the liquidus temperature as a result of undercooling. It was found by Flemings[18] that higher cooling rates result in higher undercooling.

Criteria have been developed for partitionless solidification, i.e., for solidification of a chemically homogeneous solid[16]. The constitutional supercooling criteria applies for alloys solidified under the conditions of low growth velocities and high thermal gradients, e.g., single crystals turbine blades. Essentially, the criteria states that the actual thermal gradient in the liquid must equal or exceed the slope of the liquidus curve immediately in front of the solidifying interface. At high solidification velocities, analysis of the morphological stability of the solid-liquid interface leads to the absolute stability criteria for partitionless solidification[2,19]. This analysis takes into account the effects of the solute field, the thermal field, and capillary forces. At extremely high interface velocities, the application of macroscopic transport equations are no longer valid since the interface velocity approaches or exceeds that of solute diffusion in the liquid. At these high interface velocities, solute trapping occurs and partitionless solidification is maintained.

During melt spinning, once a solid nucleates it grows rapidly. The heat of fusion reduces undercooling and slows the solid/liquid interface velocity. If the growth velocity falls below that required by the absolute stability criteria, cellular and/or dendritic microstructures result. Dendrite arm spacing and cell size adjust to reduce constitutional supercooling, i.e., faster solidification rates result in smaller spacings. Empirically, dendrite arm spacing is correlated by the cooling rate as $\delta \sim (DT/dt)^{-n}$ where the n value is in the range of 0.3 to 0.5.

HEAT TRANSFER ANALYSIS

Equations (1-5) may be solved numerically provided that all thermal properties are known and h(t) and f(T) are given. Here, a simplified heat transfer analysis, which avoids the use of h(t) and f(T), is developed to account for the process variables including material properties, the melt temperature, and the wheel temperature. The following assumptions are made in the present analysis.

(i) The heat transfer is predominantly one-dimensional in the y-direction perpendicular to the wheel.

(ii) Properties are the same for both liquid and solid and are independent of temperature. Since rapid solidification suppresses microstructural change from liquid to solid, this assumption is generally acceptable.

(iii) Both the ribbon and the wheel are considered semi-infinite plate during solidification. This is valid during the short duration of solidification on the order of one millisecond or less.

(iv) The ribbon/wheel contact is perfect during the period of solidification, i.e., contact resistance is negligible. This assumption is valid in the liquid/solid contact but may significantly overestimate heat transfer downstream of the puddle in the solid/wheel contact.

(v) Heat transfer by radiation and convection to the ambient is negligible during the short period of solidification.

(vi) Convention in molten metal is negligible as compared with the rapid motion of the wheel and ribbon. This assumption is more justified in melt extraction than in planar flow casting.

(vii) Solidification occurs at a single melting temperature, T_m. It has been shown by Flemings[18] that the majority of solidification for alloys at rapid rates takes place at a fixed temperature below the equilibrium liquidus temperature. This may be explained by the effect of undercooling mentioned above.

When the liquid metal is in contact with the wheel at t = 0, the interface temperature instantaneously takes the value of

$$T_o = \frac{T_i + T_w \beta}{1 + \beta} \tag{6}$$

and

$$\beta = \sqrt{\frac{(\rho\ c\ k)_2}{(\rho\ c\ k)_1}} \tag{7}$$

where T_i and T_w are the initial melt temperature and the wheel temperature respectively, and the subscripts "1" and "2" represent the ribbon and the wheel respectively. The value of T_o will stay

unchanged with time if both the melt and the wheel are considered semi-infinite during solidification.

Integral Solution

The surface heat flux of a semi-infinite plate with a constant surface temperature of T_o is given as,

$$q = \frac{k_1 (T_i - T_o)}{\sqrt{\pi \alpha_1 t}} \tag{8}$$

By integrating Eq. (8) over the ribbon/wheel contact time, the total heat transfer rate is,

$$Q = \int_0^t qAdt = 2k_1 A(T_i - T_o)\sqrt{\frac{t}{\pi \alpha_1}} \tag{9}$$

The heat transfer rate from Eq. (9) is used to remove the latent of fusion (solidification) and sensible heat of the superheated melt,

$$Q = \rho_l A s[L + c_l(T_i - T_m)] \tag{10}$$

Equating Eq. (9) and Eq. (10), it yields

$$s(t) = \frac{2c_l(T_i - T_o)}{[L+c_l(T_i-T_m)]\sqrt{\pi}}\sqrt{\alpha_1 t} \tag{11}$$

Exact Solution

Equation (11) overestimates the solidification thickness because it underestimates the effective specific heat due to the latent heat of fusion. If this assumption is relaxed, an exact solution may be obtained for solidification of metals with a single melting temperature[14,15]. The validity of this assumption is discussed in (vii) above. The temperature distribution in the solid region is given as:

$$\frac{T_1(x,t) - T_o}{T_m - T_o} = \frac{erf[x/2(\alpha_1 t)^{1/2}]}{erf(\lambda)} \tag{12}$$

The solidification thickness is given as:

$$s(t) = 2\lambda \sqrt{\alpha_1 t} \tag{13}$$

where λ is the root of the transcendental equation,

$$\frac{\exp(-\lambda^2)}{erf(\lambda)} + \frac{(T_m - T_i)}{(T_m - T_o)} \frac{\exp(-\lambda^2)}{erfc(\lambda)} = \frac{\lambda\sqrt{\pi} L}{c_1 (T_m - T_o)} \tag{14}$$

The cooling rate in the solid region may be obtained by differentiating Eq. (12),

$$\frac{\partial T_1(x,t)}{\partial t} = -\frac{T_m - T_o}{erf(\lambda)} \frac{x}{2\sqrt{\pi\alpha_1}} \exp\left(-\frac{x^2}{4\alpha_1 t}\right) t^{-3/2} \tag{15}$$

The solid/liquid interface velocity may be obtained by differentiating Eq. (13),

$$\frac{ds}{dt} = \lambda\, \alpha^{1/2} t^{-1/2} = \frac{s}{2t} \tag{16}$$

RESULTS AND DISCUSSIONS

Solidification Thickness, Interface Velocity, and Cooling Rate

It can be seen from Eqs. (6-16) that the effects of melt temperature, wheel temperature, and material properties on solidification phenomena are included. For example, increasing the melt temperature (and thus the superheat) decreases the interface velocity and increases the cooling rate. A wheel with higher thermal conductivity results in higher heat transfer and solidification rate. The solidified thickness is found to be proportional to the square root of time and thermal diffusivity of the ribbon. These trends are critical for developing experimental strategies and optimum operating conditions.

The following results are based on a typical experimental condition with a wheel speed of 27 m/s, a bulk wheel temperature of 550 K, and an initial molten metal temperature of 1830 K. Material properties used in the calculation are listed in Table 2 which includes ribbon materials including Al, Ti, and Al_3Ti, and wheel materials including Mo and Cu. The properties of pure elements are obtained from standard handbook. For Al_3Ti, ρ and c are based on weighted average and k is estimated using an electricity resistance measurement.

Table 2. Material Properties Used in the Analysis

Material	Al	Ti	Al_3Ti	Mo	Cu
ρ (kg/m^3)	2700	4520	3360	10240	9000
c (J/kg-K)	1180	620	980	251	503
k (W/m-K)	200	22	44	138	393
T_m (K)	983	1953	1697	-	-
L^m (kJ/kg)	390	365	385	-	-

Figure 5 shows the solidification thickness (the solid/liquid interface position) as a function of time for Al_3Ti which is melt spun on a molybdenum (Mo) wheel. It is shown that the thickness is proportional to the square root of contact time. The dashed line is calculated from Eq. (11) obtained by the integral solution. A more accurate solution is the solid line obtained from the exact solution, i.e, Eq. (13). It takes times of 0.115, 0.26, and 0.46 ms to reach thicknesses of 50, 75, and 100 μm. respectively. With a spinning speed of 27 m/s used in the experiment they correspond to lengths of 3.1, 7.02, 12.4 mm, respectively. Note that the observed ribbon length from the experiment is in the range of 5 - 15 mm.

Figure 6 shows the solid/liquid interface velocity and the cooling rate versus contact time for Al_3Ti which is melt spun on a molybdenum (Mo) wheel. The interface velocity is initially high about 0.74 m/s and is decreased to 0.11 m/s at t = 0.46 ms and a thickness (s) of 100 μm. The cooling rate is evaluated at the solid/liquid interface at the solid side (solidification front) using Eq. (14). The cooling rate is extremely high near 10^7 K/s initially and drops to 4.9×10^5 K/s at t = 0.46 ms and s = 100 μm. These values are slightly higher than those reported by Vogt[11], who showed the cooling rates for steel ribbons with thickness of 75-125 μm are in the range of $2 - 6 \times 10^5$ K/s based on infrared pyrometer measurement coupled with a 1-D finite difference model.

Figure 7 shows the comparison of interface solid/liquid interface velocity from the present analysis to that from the literature by considering a Ti ribbon spun on a Cu wheel. A wheel temperature of 300 K and a superheat of 10 K are assumed. The interface velocity versus contact time from the present analysis (solid line) is in very good agreement with that from the simulated results by Wang and Matthys[13]. The advantage of the present analysis is its simplicity wherein no numerical solution is required.

Microstructures

An optical micrograph of the ingot prior to melt spinning is

presented in Fig. 8. It clearly shows the presence of two phases: the result of solute partitioning occurring during normal solidification. X-ray diffraction and energy dispersive spectroscopy were employed in a previous study by Frazier and Benci[20] to unambiguously identify the phases. The majority phase is body centered tetragonal Al_3Ti and the minority phase (2.1 volume percent) is face centered cubic aluminum. The average grain size of the casting was measured using the line intercept method to be 125 microns. Second phase aluminum is observed within the grains and at grain boundaries. The cooling rate on the surface of the as-cast ingot measured using a ratio (two-wavelength) infrared pyrometer is around 10 K/s.

The microstructure of melt spun Al_3Ti is shown in Fig. 9. The ribbon with thickness between 80 to 100 μm exhibits two regions of distinctly different microstructures. A microcrystalline featureless region is observed near the ribbon/wheel interface and is indicative of extremely rapid growth rates and partitionless solidification. A cellular microstructure is observed near the free surface of the ribbon and is aligned in the direction of heat flow. As shown in Fig. 6, the estimated cooling rates vary from 10^7 K/s near the ribbon/wheel contact side to $5x10^5$ K/s near the free surface of the ribbon. Benci and Frazier[20] used X-ray diffraction and energy dispersive spectroscopy to interrogate the crystal structure and chemistry of the melt spun ribbon. Within the resolution of the experimental techniques, the melt spun ribbon was found chemically homogeneous and to be wholly Al_3Ti.

The DTA thermogram of melt spun Al_3Ti is presented in Fig. 10. The reactions associated with the thermal profile are somewhat complex; however, the following observations are clear: (i) the onset of melting occurs at 1354°C,(ii) the peak melting temperature is 1424°C, and (iii) the alloy is completely molten at 1469°C. These results are in reasonable agreement with those of Tarnacki and Kim[21] who report the onset of melting at 1367°C and a peak melting temperature 1414°C.

CONCLUSIONS

A one-dimensional transient mathematical model is proposed to predict the solid-liquid interface and the cooling rate. Cooling rates and solid/liquid interface velocities are calculated from an analytical solution by assuming negligible ribbon/wheel contact resistance. The resulting microstructures from a melt spun intermetallic ribbon (Al_3Ti) and a as-cast ingot of the same composition are analyzed and compared. Very fine and homogeneous microstructure is observed for the melt spun ribbon which has a cooling rate around 10^6 K/s. Nonhomogeneous microstructure with two phases and grain boundaries is noticed for the as-cast ingot which has a cooling rate around 10 K/s.

References

1. Laborsky, F. E., ed., **Amorphous Metallic Alloys**, Butterworths, London, 1983.

2. Mehrabian, R., "Rapid Solidification," International Metals Reviews, 27(4), 1982, pp. 185-208.

3. Jones, H., **Rapid Solidification of Metals and Alloys**, The Institution of Metallurgists, London, 1982.

4. Ashley, S., "Tough Materials for Tomorrow's Engines," **Mechanical Engineering**, Dec. 1991, pp. 49-52.

5. Suryanarayana, C. and Froes, F. H., "The Current Status of Titanium Rapid Solidification," **J. of Metals**, pp.22-25, March 1990.

6. Kurz, W. and Trivedi, R., "Eutectic Growth under Rapid Solidification Conditions," Metallurgical Transactions A, 22A, 1991, pp. 3051-3057.

7. Gutierrez, E. M. and Szekely, J., "A Mathematical Model of the Planar Flow Melt Spinning Process," **Metallurgical Transactions B**, Vol. 17B, pp. 695-703, 1986.

8. Takeshita, K. and Shingu, P. H., "An Analysis of the Melt Puddle Formation in the Single Roller Chill Block Casting, **Trans. Japan Institute of Metals**, Vol. 27, No. 2, pp. 141-148, 1986.

9. Berger, S. A. and Ai, D. K., "A Simple Fluid Mechanics Model for Planar Flow Casting Melt-Spinning," **Metallurgical Trans. B**, Vol. 19B, 1988, pp. 571-579.

10. Kevesh, S., "Metallic Glasses: The Technology of Rapid Solidification Processing," **Rapid Solidification Processing: Principles and Technologies**, Mehrabian, R., Kear, B. H., and Cohen, M., Eds., , Baton Rouge, 1977.

11. Vogt, E., "On the Heat Transfer Mechanism in the Melt Spinning Process," **Int. J. Rapid Solidification**, Vol. 3, pp. 131-146.

12. Muhlbach, H., Stephani, G., Sellger, R., and Fiedler, H., "Cooling Rate and Heat Transfer Coefficient during Planar Flow Casting of Microcrystalline Steel Ribbons, **International J. of Rapid Solidification**, Vol. 3, pp. 83-94, 1987.

13. Wang, G. X. and Matthys, E. F., "Modelling of Rapid Solidification by Melt Spinning: Effect of Heat Transfer in the Cooling Substrate," **Materials Science and Engineering**, A136, 1991, pp. 85-97.

14. Ozisik, M. N., **Heat Conduction**, John Wiley, New York, 1980.

15. Viskanta, R., "Heat Transfer During Melting and Solidification of Metals, **ASME J. Heat Transfer**, Vol. 110, 1988, pp. 1205-1219.

16. Flemings, M. C., **Solidification Processing**, McGraw Hill, New York, 1974.

17. Levi, C.G. and Mehrabian, R., "Heat Flow During Rapid Solidification of Undercooled Metal Droplets," Metallurgical Transactions A, 13A, 1982, pp. 221-234.

18. Flemings, M. C., Behavior of Metal Alloys in the Semisolid State," **Metallurgical Transaction B**, Vol. 22B, 1991, pp. 269-293.

19. H. Biloni, "Solidification," Physical Metallurgy, editors: R.W. Cahn and P. Haasen, Elsevier Science Publishers, New York, 1983, 478-579.

20. Frazier, W. E. and Benci, J. E., "Crystal Structure and Phase Relationships in As-Cast and Melt Spun Al3Ti and Al3Ti plus Copper," Scripta Metallurgica et Materialia, 25(10), 1991, pp. 2267-2272.

21. Tarnacki, J. and Kim, Y-W., "A Study of Rapidly Solidified Al_3Ti Intermetallics with Alloying Additions," Scripta Metallurgica, 22(11)(1988), 329-334.

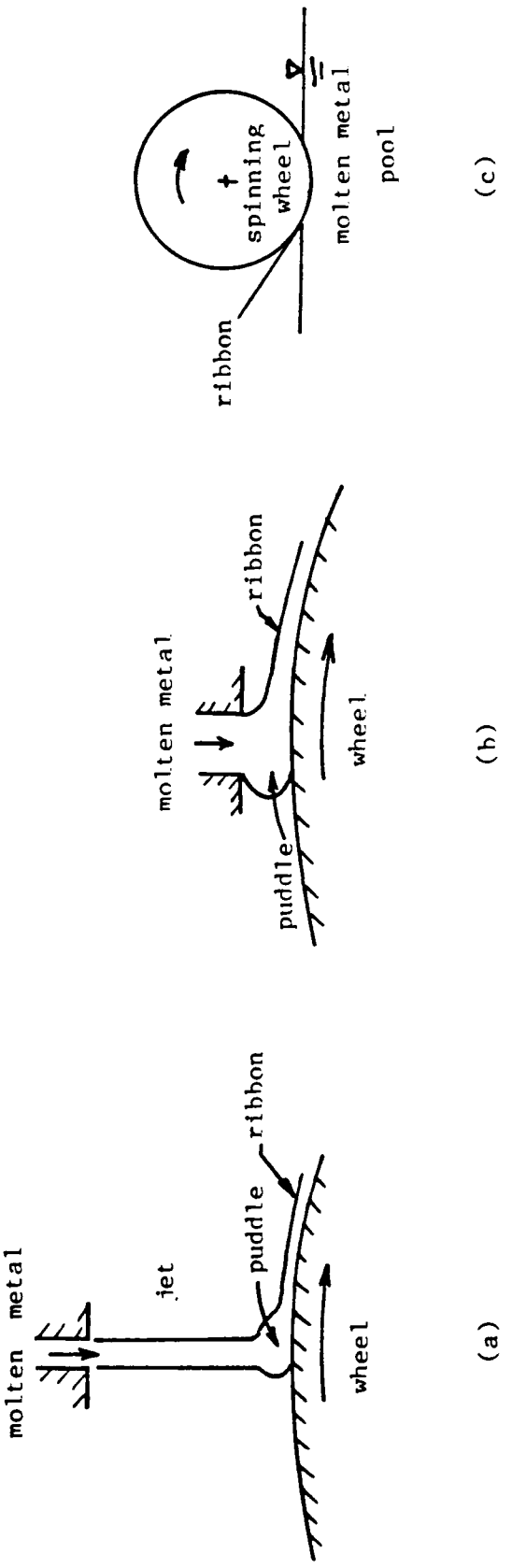

Figure 1. Three methods of melt spinning: (a) free jet melt spinning, (b) planar flow casting, and (c) melt extraction.

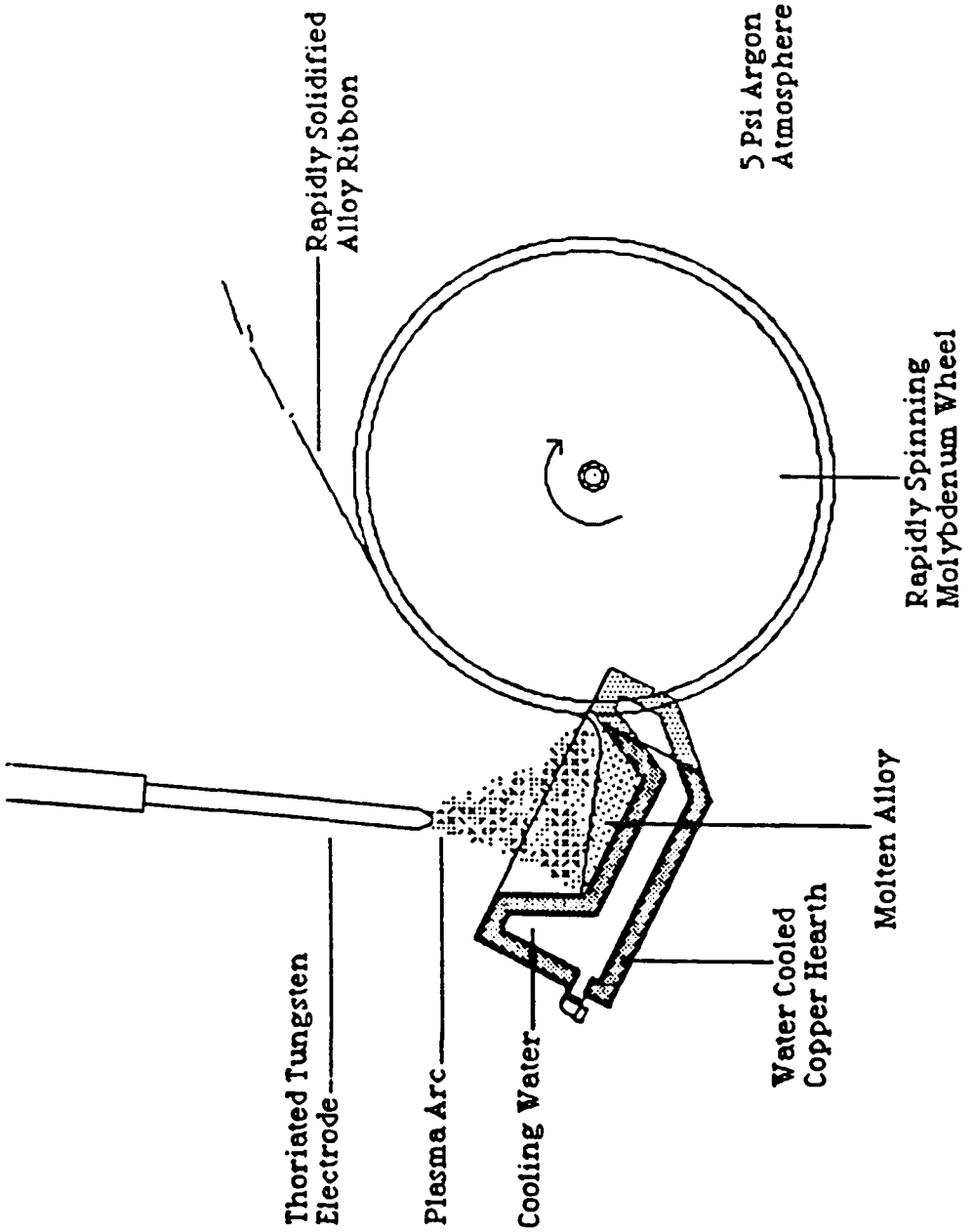

Figure 2. NAWC/AD advanced tungsten-arc melt spinner.

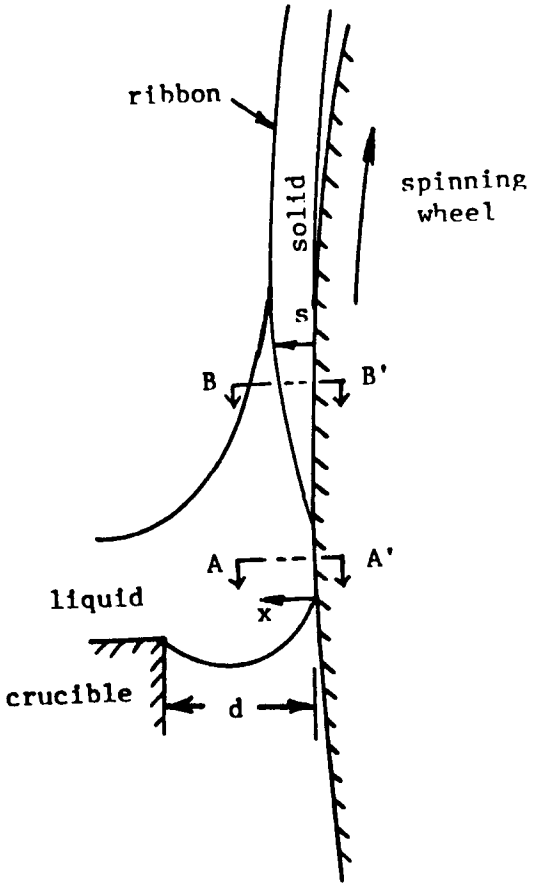

Figure 3. Schematic of the melt spinning process illustrating the anticipated fluid-solid flow morphology.

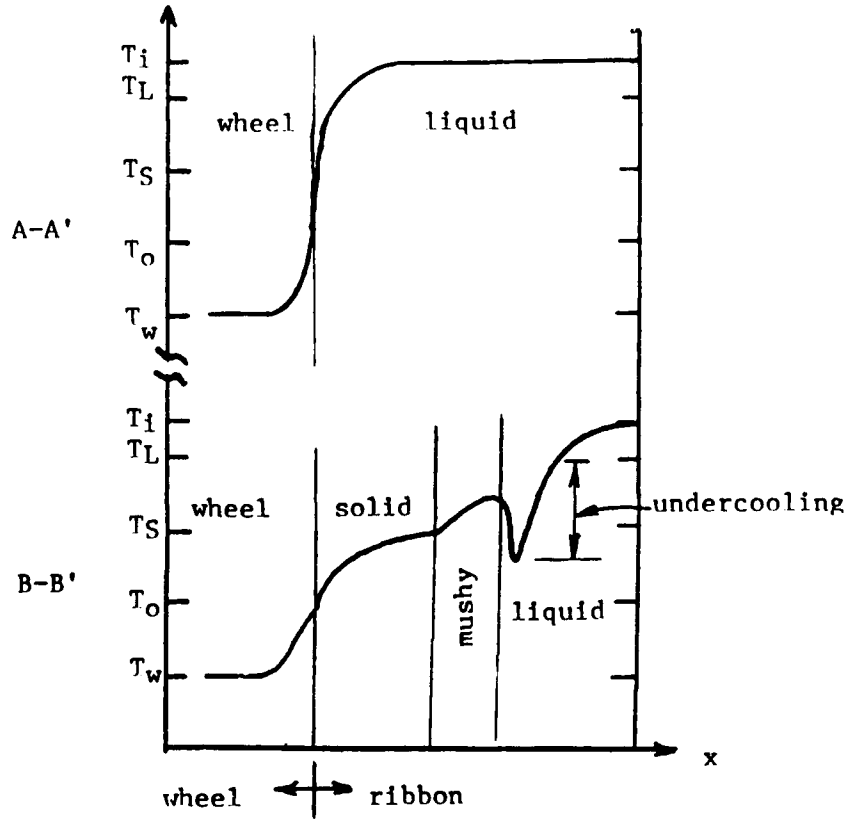

Figure 4. Temperature distributions in wheel and ribbon at two cross-sections: A-A' and B-B'.

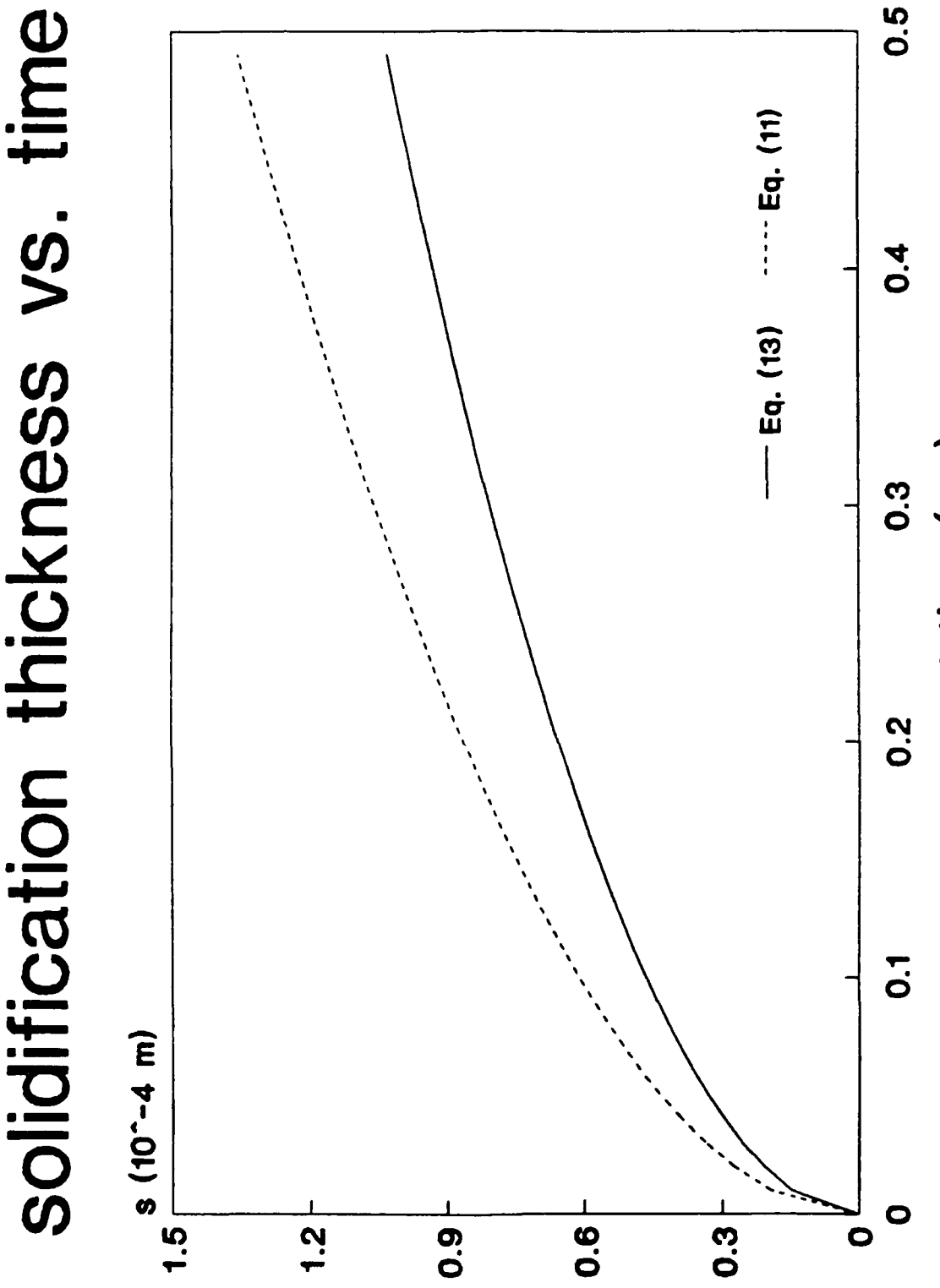

Figure 5. Solidified thickness versus contact time of Al_3Ti spun on a Mo wheel for T_i-T_m = 133 K and T_w = 550K.

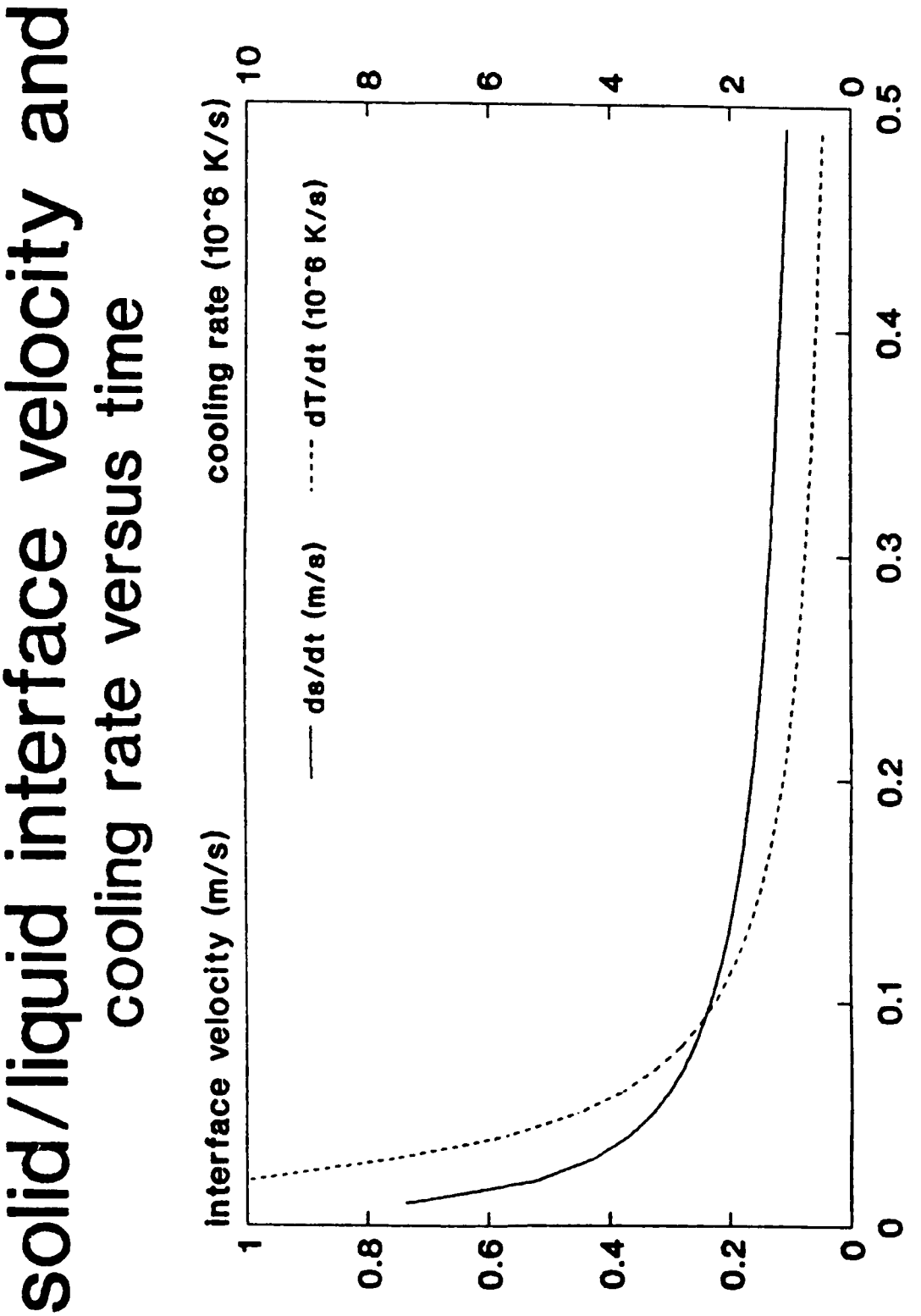

Figure 6. Solid/liquid interface velocity and cooling rate versus contact time of Al_3Ti spun on a Mo wheel for T_i-T_m=133K and T_w=550K.

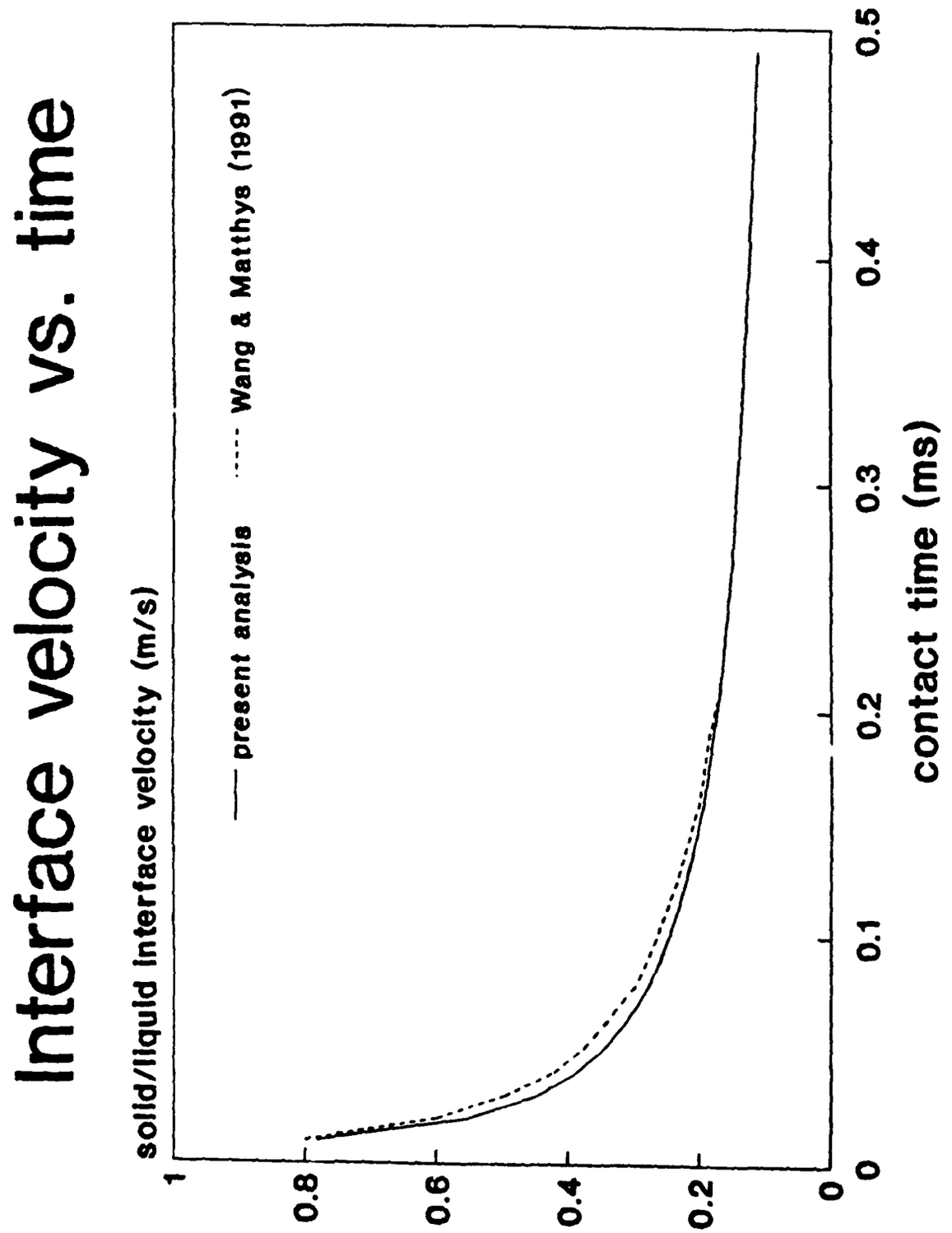

Figure 7. Solid/liquid interface velocity versus time of Ti spun on a Cu wheel for T_i-T_m=10K and T_w=300K.

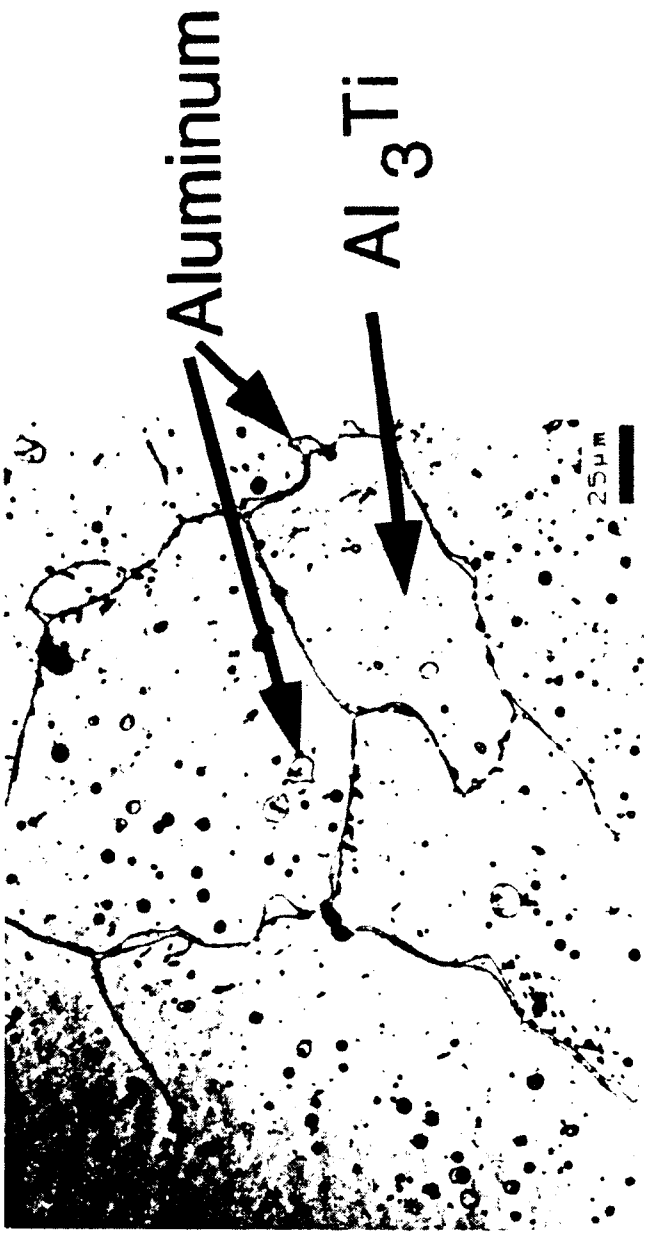

Figure 8. Optical micrograph of as-cast Al_3Ti.

FREE SURFACE

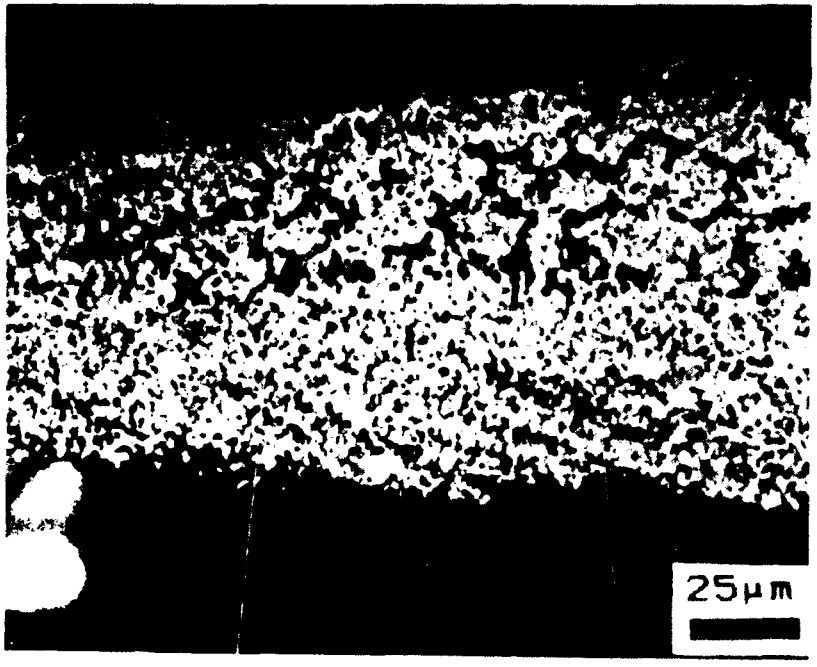

CELLULAR

MICROCRYSTALLINE

Figure 9. Optical micrograph of melt spun Al_3Ti.

WHEEL SIDE - FIRST TO SOLIDIFY

WHEEL'S ROTATION DIRECTION

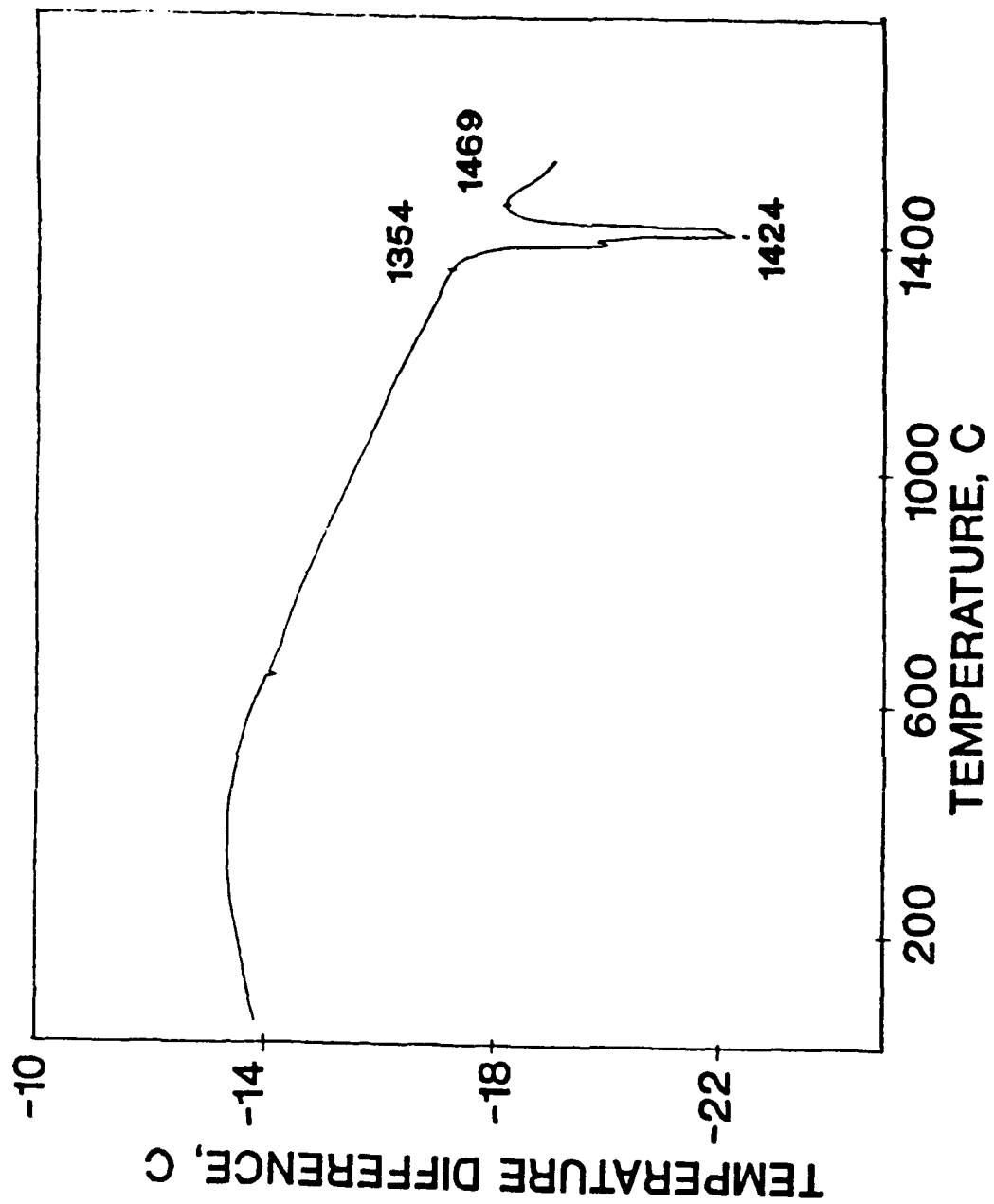

Figure 10. Differential Thermal Analysis (DTA) profile obtained for melt spun Al_3Ti.

No. of Copies

General Electric Co., Valley Forge Space Center, Phila., PA 19101.....1

Grumman Areospace Corp., Bethpage, NY 11714, M. Donnellan, P. N. Adler.....2

Howmet Corp., 1500 South Warner St., Whitall, MI 49461-1895, B. London.....1

Idaho National Engineering Laboratory, P.O. Box 1625, Idaho Falls, ID 83415, J. R. Knibloe.....1

Inco Alloys International, P.O. Box 1958, Huntington, WV 25720, J. deBarbadillo.....1

Industrial Materials Technology, P.O. Box 565, 155 River St., Andover, MA 01810, R. Widmer.....1

Innovare Inc., Airport Road, Commonwealth Park, 7277 Park Drive, Bath, PA 18014, A. R. Austen.....1

Lockheed Missiles and Space Co., Metallurgy Dept. 93-10/204, 3251 Hanover St., Palo Alto CA 94304, R. Lewis and J. Wadworth.....2

Marko Materials Inc., 144 Rangeway Rd., N. Billerica, MA 01862, R. Ray.....1

Martin Marietta Laboratories, 1450 South Rolling Rd., Baltimore, MD 21227-3898, J. Venables, K.S. Kumar.....2

Massachusetts Institute of Technology, 77 Massachusetts Av., Cambridge, MA 20139, J. Cornie.....1

Material Science Corporation, 1777 Walton Rd., Blue Bell, PA 19422.....1

McDonnell Aircraft Co., Box 516, Saint Louis, MO 63166, K. K. Sankaran.....1

MCIC, Battelle Memorial Institute, Columbus OH.....1

Metal Working News, 201 King of Prussia Rd., Radnor, PA 19089, R. R. Irving.....1

Metal Working Technology Inc. 1450 Scalp Avenue, Johnstown, PA 15904, W. L. Otto.....1

Metcut-Materials Research Group, P.O. Box 33511, Wright Patterson AFB, OH 45433, Y. W. Kim.....1

Michigan Technological University, Houghton, Michigan 49931, M. McKimpson.....1

No. of Copies

NASA Headquarters, 600 Independence Av., Washington, DC 20546, N. Mayer, S. Vennesi.....2

NASA Langley Research Center, Hampton, VA 23365, A. Taylor, L. Blackburn, J. Wagner, D. Roysten, D. Tenney.....5

National Bureau of Standards, Gaithersburg, MD 20899, R. Shaffer, J. R. Manning.....1

National Science Foundation, Office of Science and Technology Centers Division, 1800 G Street, Washington, DC 20550, L. W. Haworth.....1

NAWC/AD/WAR, Warminster, PA, 18974-5000, Library, Code 8131 (2 Copies), W.E. Frazier, Code 6063 (15 Copies).....17

NAVAIRSYSCOM, Washington, DC 20361, J. Collins Air-5304, L. Sloter Air-931.....2

NAVAIRTESCEN, Patuxent River, MD.....1

Naval Air Engineering Center, Lakehurst, NJ 08733-5100, R. Celin (AV624-2173),R. Jablonski (AV624-2174), G. Fisher (SESD) (AV624-1179), ...3

Naval Air Propulsion Test Center, P.O. Box 7176, Trenton, NJ 08628-0176, F. Warvolis (PE34), A. Culbertson, R. Mahortor.....3

Naval Air System Command, Washington, DC 20361-5140, R. A. Retta (AIR-51412), ...1

Naval Air System Command, Washington, DC 20361-5140, J. Jarrett (AIR-51412J),.....1

Naval Air System Command, Washington, DC 20361-5140, L. Sloter (AIR-931A),.....1

Naval Industrial Resources Support Activity, Bldg. 75-2 Naval Base Phila., PA 19112-5078, L. Plonsky (NAVIRSA-203).....1

Naval Industrial Resources Support Activity, Bldg. 75-2 Naval Base, Phila., PA 19112-5078, D. Fabry (NAVIRSA-204).....1

Naval Post Graduate School, Mechanical Engineering Department, Monterey, CA 93943, T. McNelly.....1

Naval Research Laboratory, Washington, DC 20375, Code 6120, Code 6306.....2

No. of Copies

Naval Ship Engineering Center, Washington DC 20360, Code 6101E,.....1

Naval Surface Warfare Center, Dahlgren, VA 22448-5000,.....1

Naval Surface Warfare Center, Silver Spring, MD 20903-5000, D. Divecha.....1

NAVAVNDEP, MCAS, Cherry Point, CA Code 340.....1

NAVAVNDEP, NAS, Alameda, CA Code 340.....1

NAVAVNDEP, NAS, Jacksonvelle, FL Code 340.....1

NAVAVNDEP, NAS, Norfolk VA Code 340.....1

NAVAVNDEP, NAS, North Island, CA Code 340.....1

NAVAVNDEP, NAS, Pensacola, FL Code 340.....1

NAVAVNSAFECEN, NAS Norfolk VA, ...1

NAVSEASYSCOM, Washington, DC 20362.....1

NAVSHIPRANDCEN, Annapolis, MD 21402.....1

NAVSHIPRANDCEN, Bethseda, MD 20034.....1

Northrop, Aircraft Division, One Northrop Av., Hawthorne, CA 90250, S. P. Agrawal and G. R. Chanani.....2

Oak Ridge National Laboratory, P.O. Box 2008, Oak Ridge, Tennessee 37831-6077, R. H. Cooper.....1

Office of Naval Research, 800 Quincy St. , Arlington, VA 22217-5000 S. Fishman Code 12, G. Yoder Code 11, J. Kelly Code OCNR-225.....3

Pratt and Whitney, P.O. Box 109600 West Palm Beach, FL 33410-9600, B. H. Walker, R. Anderson.....2

Rensselaer Polytechnic Institute, Materials Engineering Department, Troy, NY 12180-3590 N. S. Stoloff.....1

Reynolds Metals Co., Fourth and Canal St., P.O. Box 27003, A. Cho, D. Thompson.....1

Rockwell International, Science Center, 1049 Camino Dos Rios, P.O. Box 1085, Thousand Oaks, CA 91360.....1

Sandia National Laboratory, Alburquerque, NM 87185, Div. 1822 and 1832.....2

No. of Copies

Temple University, Dept. of Mechanical Engineering, 12th & Norris St., Phila., PA 19122, J. Chen.....5

Textron, 2 Industrial Avenue, Lowell, MA 01851, M. Mittnick.....1

U.S. Army Air Mobility R&D Laboratory, Fort Eustis, VA 23064, SAVDL-EU-SS.....1

University of California, Dept. of Mechanical Engineering, Irvine, CA 92717, E. J. Lavernia.....1

University of California, Dept. of Materials Science, Berkeley, CA, 94720, J. Morris, Jr., R. O. Richie.....2

University of California, Santa Barbara CA 93106, C. G. Levi.....1

University of Michigan, H.H. Dow Building, Ann Arbor, MI 48109-2136, A. Ghosh.....1

University of Pennsylvania, School of Engineering and Applied Science, 109 Town Building, Phila., PA 19104-6391, D. Pope.....1

University of Virgina, Light Metals Center, Charlottesville, VA 22901, J. Wawner, J. Wert, H. N. G. Wadley, E. A. Starke, Jr.....4

University of Wisconsin, Department of Metallurgy and Mineral Engineering, 1509 University Av., Madison, WI 53706, J. H. Perepezko.....1

U.S. Air Force, AFOSR/NE Bldg. 410, Bolling AFB, Washington, DC 20332-6448, A. H. Rosenstein.....1

USAF Systems Command, WPAFB, OH 45331.....1

Wayne State University, Detroit MI 48202, J. Benci.....2

Worcester Polytechnic Institute, 100 Institute Road, Worchester MA 01609-2280, D. Apelian.....1

DISTRIBUTION LIST
Report No. NAWCADWAR-92029-60

..... No. of Copies

Air Force Wright Aeronautical Lab.,Wrigth Patterson AFB, OH 45433, W. Griffith (MLTM), J. Kleek (WL/MLLM), and R.L. Kennard (MTM).....3

Allied-Signal Corp., P.O. Box 1021R, Morristown, NJ 07960, S.K. Das and P. Gilman.....2

Army Materials Technology Laboratory, Watertown, MA.....1

Battelle Memorial Institute, Columbus Laboratories, 505 King Av., Columbus, OH 43201.....1

BDM International, Inc., 4001 N. Fairfax Dr. #750, Arlington, VA 22203, P. A. Parrish.....1

Boeing Commercial Airplane, Seatle WA , W. Quist.....1

Boeing Corp., Aerospace Division, P.O. Box 3707, Seatle, WA 98124.....1

Boeing-Vertol Co., P.O. Box 16858, Phila., PA 19142, Dept. 1951.....1

Brookhaven National Laboratory, Department of Applied Science/PSD, Building 526, Upton, NY 11973.....1

Center for Naval Analyses, 4401 Front Ave., P.O. Box 16268 Alexandria, VA 22302-0268.....1

Clemson University, Dept. of Mechanical Engineering, Riggs Hall, Clemson, SC 29634-0921, H.J. Rack.....1

DARPA, 1400 Wilson Blvd., Arlington, VA 22209, W. Barker, B. Wilcox.....2

Defense Technical Information Center, Bldg. #5, Cameron Station, Bldg. 5, Alexandria, VA 22314 (Attn. Adminstrator).....2

Department of Energy, 100 Independence Av., SW Washington, DC 20585, Code CE142.....1

Drexel University, Dept. of Materials Engineering, 32nd and Chestnut St., Phila., PA 19104, M. J. Koczak 1

Garrett Auxiliary Power Division, 2739 East Washington Street, P.O. Box 5227, Phoenix, AZ 85010, C. McCormick.....1